

The radial distribution of supernovae compared to star formation tracers

Fiona M. Audcent-Ross,^{1*} Gerhardt R. Meurer,¹ James R. Audcent,² Stuart D. Ryder,³ O.I. Wong,^{1,4} J. Phan,² A. Williamson,⁵ and J.H. Kim^{6,7}

¹ *International Centre for Radio Astronomy Research, University of Western Australia, 35 Stirling Highway, Crawley, WA 6009, Australia*

² *University of Western Australia, 35 Stirling Highway, Crawley, WA 6009, Australia*

³ *Department of Physics and Astronomy, Macquarie University, Sydney, NSW 2109, Australia*

⁴ *ARC Centre of Excellence for All Sky Astrophysics in 3 Dimensions (ASTRO 3D), Australia*

⁵ *Curtin University, Kent Street, Bentley, WA 6102, Australia*

⁶ *Subaru Telescope, National Astronomical Observatory of Japan, 650 North A'ohoku Place, Hilo, HI 96720, USA*

⁷ *Metaspaces, 36 Nonhyeon-ro, Gangnam-gu, Seoul, 06312, Republic of Korea*

Accepted xx. Received YYY; in original form ZZZ

ABSTRACT

Given the limited availability of direct evidence (pre-explosion observations) for supernova (SN) progenitors, the location of supernovae (SNe) within their host galaxies can be used to set limits on one of their most fundamental characteristics, their initial progenitor mass. We present our constraints on SN progenitors derived by comparing the radial distributions of 80 SNe in the SINGG and SUNGG surveys to the *R*-band, $H\alpha$, and UV light distributions of the 55 host galaxies. The strong correlation of Type Ia SNe with *R*-band light is consistent with models containing only low mass progenitors, reflecting earlier findings. When we limit the analysis of Type II SNe to apertures containing 90 per cent of the total flux, the radial distribution of these SNe best traces far ultraviolet (FUV) emission, consistent with recent direct detections indicating Type II SNe have moderately massive red supergiant progenitors. Stripped Envelope (SE) SNe have the strongest correlation with $H\alpha$ fluxes, indicative of very massive progenitors ($M_* \gtrsim 20 M_\odot$). This result contradicts a small, but growing, number of direct detections of SE SN progenitors indicating they are moderately massive binary systems. Our result is consistent, however, with a recent population analysis suggesting binary SE SN progenitor masses are regularly underestimated. SE SNe are centralised with respect to Type II SNe and there are no SE SNe recorded beyond half the maximum disc radius in the optical and one third the disc radius in the ultraviolet. The absence of SE SNe beyond these distances is consistent with reduced massive star formation efficiencies in the outskirts of the host galaxies.

Key words: supernovae: general

1 INTRODUCTION

The number of supernovae (SNe) being detected has increased significantly in the past decade (e.g. Lennarz, Altmann & Wiebusch 2012; Gal-Yam et al. 2013) due to the

detection of fainter SNe and expanding automated monitoring programs (e.g. Bloom et al. 2012a; Magnier et al. 2013; Masci et al. 2017; Bellm et al. 2019). There is, however, only a small number of nearby SNe cases for which the SN progenitor has been directly identified (see references in Smartt 2015; Van Dyk 2017).

Given limited direct evidence on the nature of SN progenitors, various researchers are using indirect methods to constrain key progenitor characteristics, such as mass and metallicity. Examining both the host galaxy and the local environment in which SNe have occurred has, therefore, become important. Stars, particularly massive ones,

* E-mail: fiona.audcent-ross@icrar.org

are believed to form in clusters (e.g. Lada & Lada 2003; Bressert et al. 2010) and, given low typical velocity dispersions (e.g. Bastian & Goodwin 2006; Portegies Zwart, McMillan & Gieles 2010), massive SN progenitors will therefore end their short lives in, or not far from, their birthplace environments. Recent indirect methods used to study SN progenitors include examining the radial distributions of the SN population (e.g. Bartunov, Marakova & Tsevetkov 1992; van den Bergh 1997; Anderson & James 2009), analysing and modelling SN light curve behaviour (e.g. Fryer et al. 2010; Gonzalez-Gaitan et al. 2015) and dating the stellar populations near the SN location (e.g. Gogarten et al. 2009; Kuncarayakti et al. 2013b; Lyman et al. 2018; Maund 2018). This work uses the radial aperture analysis method (see Section 2.2) to gain insights into the likely progenitor masses of key SN types.

Supernovae fall into two broad categories: Type Ia SNe and core collapse supernovae (CCSNe). CCSNe occur at the end of the main sequence life of massive stars ($M \gtrsim 8 M_{\odot}$) when exothermic fusion in the core ceases, leading to the rapid gravitational collapse of the core and subsequent explosive ejection of the outer layers of the star (Bethe et al. 1979). Either a neutron star or a black hole is formed, dependent on the stellar mass of the progenitor at the point of collapse (Heger et al. 2003).

SNe are classified according to their spectral properties (see Minkowski 1941; Filippenko 1997; Gal-Yam 2016, and references therein), with Type II CCSNe having hydrogen lines, unlike Types Ib and Ic. The diversity of CCSNe types is believed to reflect the extent of the progenitor’s hydrogen envelope retained at the time of explosion. Type Ib spectra contain helium lines, but Type Ic have neither hydrogen nor helium spectral features, having experienced the loss of their outer layers. Immediately after exploding, a Type IIb SN exhibits spectral features similar to a Type II CCSN but the hydrogen lines in the spectra disappear quickly (often within weeks) and the observed spectra is then typical of a Type Ib (e.g. Filippenko, Matheson & Ho 1993). Prompt observation of SN spectra is, therefore, essential for accurate distinction between these related SN types (e.g. Maund et al. 2004). Type IIb SN progenitors are thought to retain as little as $0.01 M_{\odot}$ of their hydrogen envelopes at the time of exploding (Taddia et al. 2018), explaining the short-lived hydrogen spectral features. Stripped-envelope supernova (SE SNe: Types Ib, Ic, Ib/c and IIb) are grouped together in this paper, as these spectrally-related objects are expected to have similar progenitor channels (e.g. Arcavi et al. 2012).

Type II CCSNe can also be classified according to the shape of their light curves in the weeks after going supernova; cases where the light curve drops linearly are classified IIL while the more common Type IIP feature a plateau phase. There is, however, growing support for the view that Types IIL and IIP, as originally defined, are part of a larger continuous distribution (see discussion in Sanders et al. 2015).

For a star to terminate as a SE SN it must lose its outer layers of hydrogen (for a Type Ib) and, for Type Ic, also its layers of helium. See Smith (2014) for a review of mass loss in SE SN progenitors. This mass loss could arise from one of the following proposed mechanisms, or a combination of them: mass transfer to a nearby companion (e.g. Crockett et al. 2007; Smith et al. 2011b; Eldridge et al. 2015), ejection

of a common envelope in a binary system (Podsiadlowski, Joss & Hsu 1992), precursor luminous blue variable (LBV) eruptions (Smith & Owocki 2006; Kotak & Vink 2006; Groh, Meynet & Ekström 2013a; Smith, Mauerhan & Prieto 2014), pulsation-driven superwinds in red supergiants (Heger et al. 1997), or strong winds in Wolf-Rayet (WR) stars (Begelman & Sarazin 1986; Gaskell et al. 1986).

Beyond the Local Group, Type Ia SNe are the primary distance probes used by astronomers (Phillips et al. 1999) and have played a pivotal role in the discovery of the accelerating expansion of the Universe (Riess et al. 1998). These extremely bright thermonuclear explosions are thought to arise from the destruction of mass-accreting or merging carbon-oxygen white dwarfs (WDs: Hoyle & Fowler 1960; Hillebrandt & Niemeyer 2000). Type Ia SNe have strong ionized silicon lines in their spectra and, unlike CCSNe, have no hydrogen or helium lines, indicating that the progenitors are not main sequence stars.

Despite their importance, the progenitors for Type Ia remain subject to conjecture, with no direct detections to date and several possible progenitor models under consideration (see Livio & Mazzali 2018, for a recent review). In the single degenerate (SD) model the WD progenitor gains mass through accretion from a non-degenerate companion (either a red giant or main sequence star) and, upon reaching the Chandrasekhar limit ($M_{\text{Ch}} \approx 1.4 M_{\odot}$: Chandrasekhar 1931; Stoner 2011), explodes (e.g. Whelan & Iben 1973; Nomoto 1982; Nomoto & Leung 2018). Different variants on the SD model include a range of masses and evolutionary states for the companion and a range of WD progenitor masses: below, at, or above M_{Ch} (e.g. Nomoto, Thielemann & Yokoi 1984; Han & Podsiadlowski 2004; Howell et al. 2006; Hachisu et al. 2012; Shen et al. 2018a; Goldstein & Kasen 2018). In the double-degenerate (DD) model, two low mass WDs in a binary system merge due to gravitational interaction (Iben & Tutukov 1984; Webbink 1984), taking the combined mass over the Chandrasekhar limit (Howell 2011).

In order to constrain progenitor properties by location within the host, it is important to start with a well selected sample of potential host galaxies. The potential host selection criteria should be homogeneous and well stated so that the inevitable biases can be identified. Anderson & James (2009), for example, note that their heterogeneous sample has an increased bias towards brighter SNe and brighter galaxies.

Surveys based on optically selected potential hosts are estimated to miss up to 20 per cent or more of SNe in the local Universe (e.g. Mattila et al. 2012; Jencson et al. 2019), with increasing fractions missed at higher redshifts due to high extinction from dust. Extinction can be extreme, for example, in the luminous infrared galaxies (LIRGs) that dominate star formation at higher redshifts (Kool et al. 2018). Locally, dust in the bars and bulges of galaxies will preferentially obscure optically dim SNe (Cappellaro, Evans & Turatto 1999; Botticella et al. 2012; Horiuchi et al. 2011). Resolving new point sources arising from SN events in or near the very luminous centres of galaxies can also be difficult, especially where there is a strong flux gradient (e.g. Cappellaro et al. 1997). Saturation of detectors by nuclei can be problematic and can cause central SNe to be missed at optical wavelengths (e.g. Kool et al. 2018).

Galaxy-targeted surveys are biased against low mass

and low luminosity galaxies (Botticella et al. 2012), despite them making an important contribution to the total star formation occurring in the local Universe (Audcent-Ross et al. 2018).

Here we examine the constraints we can place on SN progenitors using a sample of potential host galaxies selected by atomic hydrogen (HI) content in the very local Universe, and observed with star formation tracers in the optical and ultraviolet. Specifically, our base of potential hosts is the galaxies observed for the Survey for Ionised Neutral Gas Galaxies (SINGG; Meurer et al. 2006), and the Survey of Ultraviolet emission in Neutral Gas Galaxies (SUNGG, Wong et al. in prep). These surveys are discussed further in Section 2.4.

The paper is organised as follows: Section 2 presents our method, starting with the rationale behind it in Section 2.1. Section 2 then explains the radial aperture analysis method in detail and outlines the two surveys and the SN sample used in this work. Section 3 shows that the radial distribution of SNe is consistent with Type Ia progenitors having low mass companions; Type II progenitors have masses at the lower end of the mass range traced by FUV; and SE SNe originate from high mass stars. These results are discussed further in Section 4. We present our conclusions in Section 5.

A Hubble constant of $H_0 = 70 \text{ km s}^{-1} \text{ Mpc}^{-1}$ and cosmological parameters for a Λ CDM cosmology of $\Omega_0 = 0.3$ and $\Omega_\Lambda = 0.7$ have been used throughout this paper.

2 THE RADIAL APERTURE ANALYSIS METHOD AND OUR SAMPLE

2.1 The rationale

Within late type galaxies the distance from an object to the galactic centre is a useful proxy for the likely local environment of that object. Stars located centrally are, for example, more likely to be associated with the central bulge, normally comprising older, higher metallicity stellar populations (e.g. Larson 1976; Peletier & Balcells 1996; Driver et al. 2006). Conversely, stars located further from the galactic centre are more likely to be in the stellar disc and to be associated with the younger stellar populations dominating the galaxy’s spiral arms (e.g. Smith 1968). Radial aperture analysis compares the radial locations of SNe to the radial fluxes of host galaxies, giving insights into which stellar populations host SN progenitors. Radial flux distributions can be impacted by internal and external factors, however, and these need to be considered when interpreting results. The actions of a strong bar, for example, can reduce local massive star formation (e.g. Hakobyan et al. 2016a) and minor mergers or interactions can trigger considerable localised star formation (e.g. Bushouse 1987; Bastian et al. 2005; Bekki 2008), significantly altering radial flux distributions.

2.2 The method

Radial aperture analysis (James & Anderson 2006; Anderson & James 2009) uses the total detectable optical and UV fluxes for a given galaxy using a curve of growth approach.

Galaxy fluxes are measured within concentric elliptical apertures, centred on the galactic centre, out to the maximum radius at which light is detected above sky levels (for further detail see Meurer et al. 2006). The elliptical aperture enclosing the total detectable flux of the host galaxy (having a radius $R = R_{\text{max}}$; see Meurer et al. 2018) is then scaled down to determine the smaller, concentric ellipse that intersects with the individual SN (see Fig. 1). The ratio of the flux contained within the SN-enclosing ellipse to the total flux of the galaxy provides a useful measure of the supernova’s centralisation. A SN located at the host galaxy’s centre has a radial enclosed flux fraction of zero, while a SN located at R_{max} has a radial enclosed flux fraction of 1. Here we use four different radial flux distributions to derive a cumulative distribution function (CDF) of the flux contained within SN locations. Specifically, the four fluxes used are the R -band continuum and $H\alpha$ from SINGG and the near and far ultraviolet (hereafter NUV and FUV) from SUNGG. A 1:1 CDF is indicative of an excellent radial tracer for the SN type under consideration.

This work utilises CDFs derived over two ranges; firstly, over the entire radial profile of the galaxy (R_{max}) and, secondly, out to R_{90} , where only 90 per cent of the total flux is contained. Using R_{90} allows the bulk of the light to be assessed, while ignoring the outer regions where star formation can be significantly different due to local environmental factors. Large changes in local star formation efficiency (SFE, the ratio of star formation rate relative to the available gas supply) in the outer disc may reflect areas where local gas surface densities fall below critical star formation thresholds (Kennicutt 1989; Roškar et al. 2008), or changes in disc stability (e.g. Martin & Kennicutt 2001), accretion of cold gas from outside the disc (Sancisi et al. 2008; Wang et al. 2018), or possible changes in the IMF (see Section 4.2). Sufficiently large changes in SFE will generate a break in the typically exponential form of a spiral galaxy’s surface brightness profile (Patterson 1940; Freeman 1970; Zheng et al. 2015). In SINGG, R_{90} typically lies just beyond where breaks in the basic exponential form occur (Zheng et al. 2015; Meurer et al. 2018, break radius $R_B \sim 0.75 R_{90}$).

R -band, $H\alpha$, NUV and FUV CDFs are used as these fluxes are sensitive to different but overlapping mass ranges of stars, allowing us to constrain possible mass ranges for SN progenitors. $H\alpha$ is an excellent direct tracer of very high mass star formation ($M_* \gtrsim 20 M_\odot$), as only the most massive, short-lived ($t < 10 \text{ Myr}$) O-type stars, are able to give rise to the photoionization of HII regions, leading to recombination $H\alpha$ emission. R -band is a good tracer of stars, covering the entire mass spectrum down to $\leq 1 M_\odot$. UV emission arises from both O- and B-type stars. It is a useful indicator, therefore, of recent star formation of high mass stars ($M_* \gtrsim 3 M_\odot$). For further explanation on the mass sensitivities of $H\alpha$ and FUV emission see Section 3.1 of Meurer et al. (2009).

2.3 An inclination cut

Assuming circularity of disc galaxies, elliptical apertures arise from the inclination of the host galaxy with respect to the plane of the sky. Line of sight issues are most extreme for galaxies with a large inclination value. Fluxes are measured using concentric elliptical apertures, regardless of the host’s

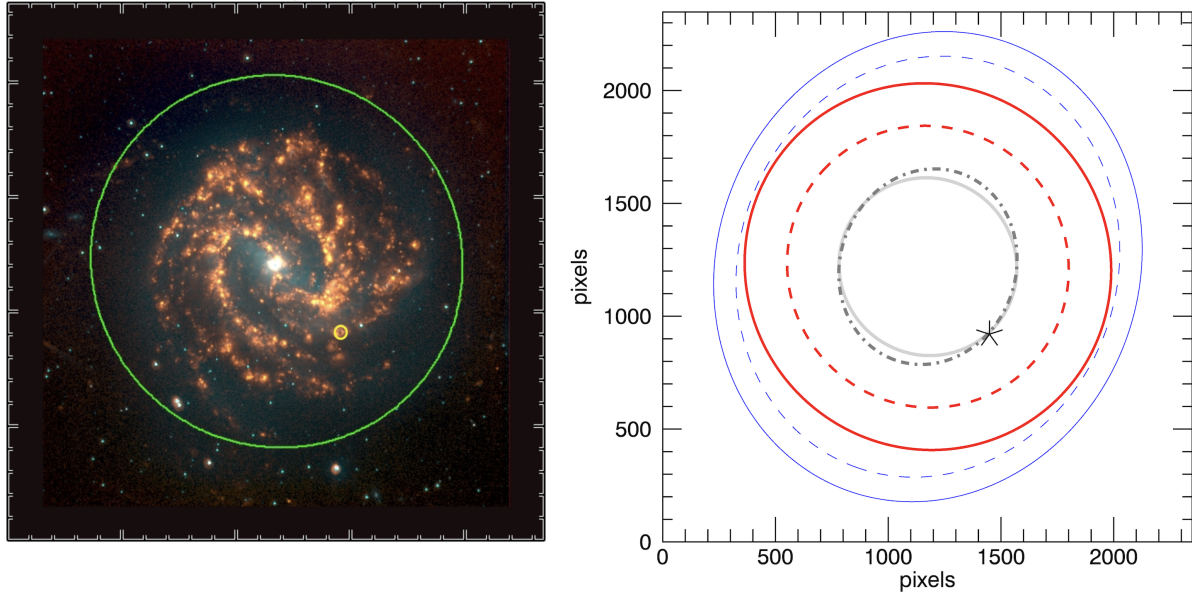


Figure 1. SN 1983N and host galaxy J1337-29 (M83). *Left:* A three-colour image of J1337-29 with a yellow open circle indicating the location of SN 1983N inside the elliptical R -band flux aperture (of radius $R = R_{\max}$, Meurer et al. 2018). R -band flux is displayed in blue, narrow-band H α (before continuum subtraction) in green and net H α (narrow-band H α post continuum subtraction) in red. North is up, east is to the left and the minor tick marks are 100 pixels (43") apart. *Right:* SN 1983N is indicated with a star and the R -band and FUV R_{\max} apertures for the host galaxy are indicated with thick red and blue ellipses, respectively. The concentric apertures containing 90 per cent of the R -band and FUV fluxes are indicated with red and blue dashed ellipses, respectively. The thick light grey solid line indicates the SN-enclosing aperture concentric with optical apertures and the thick dash-dot dark grey line marks the SN-enclosing aperture concentric with FUV apertures. Note that the optimal SUNGG UV and SINGG optical apertures were determined independently, generating very similar, but not always identical, apertures (size, ellipticity and position angle). Differences in ellipticity and position angle are generally small and immaterial, as seen here. For an overview of the differences in aperture sizes see Figure 2.

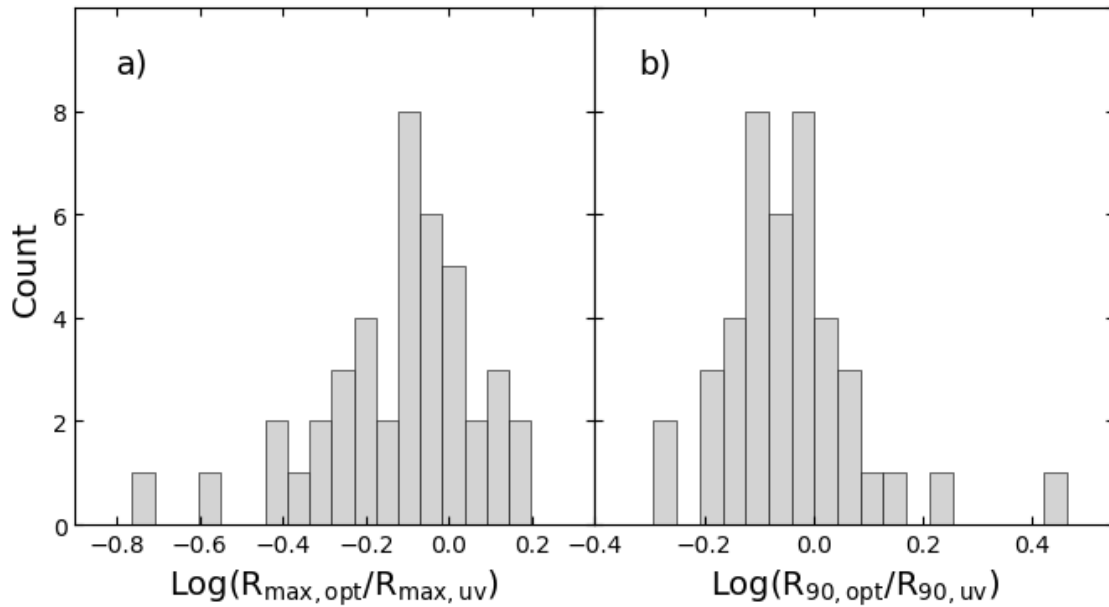


Figure 2. Comparison of SINGG (optical) and SUNGG (UV) elliptical flux measurement apertures at: (a) R_{\max} and (b) R_{90} . The 42 SNe host galaxies common to SINGG and SUNGG include many with an extended UV (XUV) disc in comparison to their optical disc (Thilker et al. 2007).

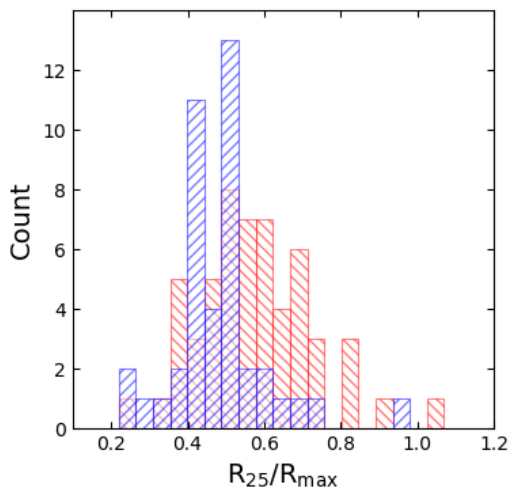


Figure 3. Comparison of SINGG R -band (red) and SUNGG FUV (blue) flux measurement apertures (R_{\max}) with R_{25} , the isophote at which the surface brightness of the host galaxy reduces to 25.0 mag per square arcsecond (measured in the B -band). The 55 SNe hosts have optical and, where applicable, UV apertures that are consistently larger than R_{25} , with median R_{25}/R_{\max} ratios of 0.55 and 0.49, respectively. R_{25} values have been obtained from NED; if multiple measurements were available the first-listed value in NED has been used.

inclination. Light from highly inclined galaxies generally require very large corrections for extinction due to dust and, as a result, less luminous supernovae can remain undetected in these galaxies (Mattila et al. 2012). Only host galaxies meeting an axial ratio criterion ($a/b < 4$) were, therefore, used in our analysis.

Line of sight considerations may bias apparent SN positions towards being more centralised than they really are. In theory, a SN that appears to be centrally located could, for example, actually be part of the outer bulge stellar populations or the surrounding, more distant, halo. This is unlikely to be a major issue, however, given very few SNe are located in galactic bulges (e.g. Johnson & MacLeod 1963; Hakobyan et al. 2016a, 2017). In a review of 500 SNe in local non-disturbed galaxies Hakobyan et al. (2016a), for example, found all the CCSNe and the vast majority of Type Ia SNe were located in the disc, rather than in the bulge or halo components of the host galaxies.

Despite the caveats outlined above, the radial distribution of historical SNe has been useful, identifying differences in SN distributions by type and providing insights into both CCSNe and Type Ia progenitors (e.g. Bartunov et al. 1992; Wang, Höflich & Wheeler 1997; Ivanov, Hamuy & Pinto 2000; Bartunov, Tsvetkov & Pavlyuk 2007; Förster & Schawinski 2008; Anderson & James 2009).

2.4 The SINGG and SUNGG surveys

SINGG and SUNGG are surveys of star formation in a sample of HI-selected galaxies selected from the HI Parkes All-Sky Survey (HIPASS: Meyer et al. 2004; Zwaan et al. 2004; Koribalski et al. 2004), using $H\alpha$ and UV emission as trac-

ers of star formation, respectively. SINGG (Meurer et al. 2006) observed 288 HIPASS sources revealing 466 galaxies with $H\alpha$ emission (at rest $\lambda = 6562.82 \text{ \AA}$) using a variety of narrow band filters, and primarily a broad R -band filter for continuum characterisation and subtraction. Sources were selected to fully sample the HI mass function in order to obtain a complete view of star formation in the local Universe. See Meurer et al. (2006); Hanish et al. (2006); Audcent-Ross et al. (2018) and Meurer et al. (2020 in prep.) for further discussion.

SUNGG (Wong 2007; Wong et al. 2016) uses GALEX NUV (central wavelength $\lambda_c = 2273 \text{ \AA}$) and FUV ($\lambda_c = 1515 \text{ \AA}$) observations of 418 unique galaxies with HI previously detected by HIPASS. Only HIPASS sources meeting the axial ratio criterion $a/b < 4$ were used in SUNGG, as highly-inclined galaxies can experience severe extinction of their UV fluxes due to dust located in the plane of the host galaxy. There are 231 HIPASS sources containing 320 star forming galaxies in common between the two surveys.

The surveys have been used to measure the local star formation rate density, highlighting the importance of the contributions made from galaxy types that can be under-represented in optically-selected samples: low HI mass, low luminosity and low surface brightness galaxies (Hanish et al. 2006; Audcent-Ross et al. 2018). Evidence of possible reduced massive star formation has been detected in low luminosity and low surface brightness galaxies as well as in the outskirts of galaxies (Meurer et al. 2009; Bruzese et al. 2015; Watts et al. 2018; Bruzese et al. 2019).

A common measure of a galaxy’s radius is R_{25} , the isophote at which the surface brightness of the galaxy measured in the B -band reduces to 25.0 mag per square arcsecond. R_{25} values for the host galaxies of our sample were extracted from the NASA/IPAC Extragalactic Database (NED), using the first-listed value in NED, if multiple measurements were recorded. SINGG and SUNGG apertures are, on average, double the R_{25} values (see Fig. 3). The SINGG and SUNGG surveys are designed to measure the star formation rate density of the local universe and so the optical and UV elliptical apertures are set to ensure *all* detectable fluxes from the target galaxy are included. This was achieved using a curve of growth analysis to capture all the detectable optical and UV fluxes, respectively. As the optimal SUNGG UV and SINGG optical apertures are determined independently they are not always identical in size, ellipticity and position angle (see Fig. 1b). The SINGG apertures (both R_{\max} and R_{90}) for the host galaxies are typically smaller than their SUNGG UV counterparts (see Fig. 2), consistent with many of these local galaxies having significantly extended UV discs (Thilker et al. 2005, 2007).

2.4.1 Non-stellar sources of $H\alpha$ and FUV emission

Galactic $H\alpha$ emission does not solely arise from massive star formation (see Vučetić, Arbutina & Urošević 2015, for a review of contaminating sources); shocks (e.g. Kenney et al. 2008), active galactic nuclei (AGN), planetary nebulae and supernova remnants (SNR), for example, can generate $H\alpha$ emission. Vučetić et al. (2015) measured the contribution of the observed SNR $H\alpha$ emission to the total $H\alpha$ flux for 25 very local galaxies that contain optically detected SNR, finding SNR generate 0.2–12.8 per cent of the total $H\alpha$ fluxes.

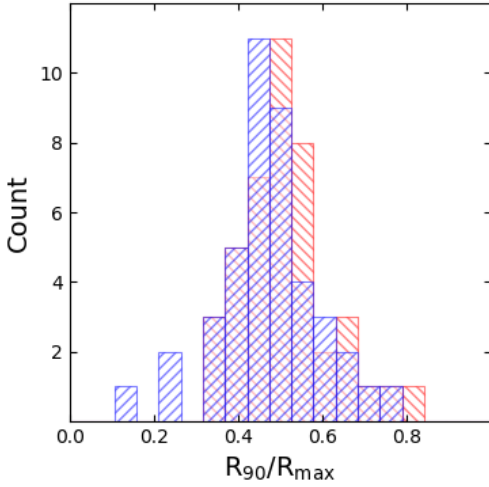


Figure 4. Comparison of SINGG R -band (red) and SUNGG FUV (blue) compactness (R_{90}/R_{\max}) values for the 42 host galaxies with both SINGG and SUNGG observations. The low average compactness values reflect the significant centralisation of the R -band and FUV fluxes (centred on $R_{90}/R_{\max} \sim 0.5$).

Due to selection effects the measurements represent lower limits. Two SINGG galaxies in our sample were examined by Vučetić et al. (2015); J2357-32 (NGC 7793) has a small measured SNR contribution of 1 per cent of total $H\alpha$ emission from 27 SNR, while 296 known SNR in J1337-29 (M83) contribute 9 per cent of its total $H\alpha$ emission. The spatial distribution of SNR (e.g. Lee & Lee 2014; Anderson et al. 2017) in the 55 SINGG hosts could impact on the $H\alpha$ CDF, but allowing for this complication is beyond the scope of this current work.

Eight host galaxies (containing 13 SNe) are classified as Seyferts. The AGN impact on the radial flux distributions of the hosts has been ignored in our analysis, even though AGN may generate considerable central $H\alpha$ and FUV fluxes (e.g., Sullivan et al. 2000; Driver et al. 2018). However, the $H\alpha$ flux emission from an AGN is typically dwarfed in comparison to emission at larger radii (e.g. Sullivan et al. 2000; Driver et al. 2018).

2.5 The supernova sample

The IAU Central Bureau for Astronomical Telegrams (CBAT) listing¹, David Bishop’s “Latest Supernovae” website², and the Open Supernova Catalog³ (Guillochon et al. 2017) were searched (all last accessed/downloaded 27th May 2019), by SN coordinates and host name, to identify recorded SNe that had potentially occurred within the galaxies of the SINGG and SUNGG surveys. This approach was used to alleviate any potential bias against extreme outlying known SNe. Targeted surveys using very limited fields of view will, however, generate a bias against the detection

of extreme outlying SNe. See Section 1 for more discussion on survey biases.

All events in these catalogues known not to be a SN were ignored for this study. The 466 star-forming galaxies of SINGG contain 101 known SNe, including 18 of uncertain type. The SNe of unknown type are excluded from the radial aperture analysis. Three host galaxies (J0953+01, J1445+01 and J1513-20) failed the axial ratio criterion ($a/b < 4$: see Section 2.2) and the SNe located therein (1983E, 1983P, and 2002ds, respectively) are, therefore, also excluded from the analysis.

The 80 SNe in our final sample represent all the most common types (see Graur et al. 2017), while rarer types, including Type IIn SNe (e.g. Cappellaro et al. 1997), were not found. There are 62 CCSNe and 18 Type Ia SNe and these are located at distances of 4–128 Mpc. Type Ia SNe occur in both early and late types of galaxies, but the SINGG sample contains few early-type galaxies; the HI-selection of the SINGG and SUNGG samples biases against early-type galaxies which typically have negligible or low levels of HI and star formation.

3 RESULTS

3.1 Type Ia: A central deficit

The radial distribution of Type Ia SNe in Figure 5a is best traced by the R -band and $H\alpha$ light distributions (Kolmogorov-Smirnov (KS) $p = 0.69$ and 0.81 , respectively). The R -band CDF for Type Ia SNe generally lies below the normal line in the inner region (Fig. 5a), however, indicating a relative central deficit of SINGG Type Ia SNe with respect to R -band flux (see also Fig. A1a); only ~ 11 per cent of Type Ia SNe are located within the inner 20 per cent of the total R -band flux, for example. This is consistent with observations by other researchers. Anderson et al. (2015b), for example, used a much larger sample of 102 Type Ia SNe in star-forming galaxies and identified reduced numbers of Type Ia SNe within the inner 20 per cent of R -band emission.

In early work Whipple (1939) observed that SNe traced stellar luminosity, with a possible tendency to “avoid the nucleus” and the central deficit of Type Ia SNe in late type galaxies is well-known (e.g. Wang, Höflich & Wheeler 1997; Tsvetkov, Pavlyuk & Bartunov 2004; Bartunov, Tsvetkov & Pavlyuk 2007, Anderson et al. 2015b). In elliptical hosts the distribution of Type Ia SNe traces the overall galaxy light profile, albeit with a lower SNe rate per unit mass, and no central deficit is observed (e.g. Bartunov et al. 2007; Förster & Schawinski 2008). Similarly, fewer Type Ia SNe per unit mass are produced in bulges compared to the discs of spiral galaxies (e.g. Anderson et al. 2015b; Hakobyan et al. 2016b), resulting in the conclusion that the vast majority of Type Ia SNe are located in the disc, and not in the bulge or halo components, of their hosts (e.g. Johnson & MacLeod 1963; Hakobyan et al. 2017). As the bulges of late type galaxies typically contribute approximately 30 per cent of the total R -band flux (e.g. Morselli et al. 2017) but produce fewer Type Ia SNe per unit mass, the central values of the R -band CDF for Type Ia SNe are lower than the normal line, as observed in SINGG (Fig. 5a).

¹ <http://www.cbata.harvard.edu/lists/Supernovae.html>

² <http://www.rochesterastronomy.org/supernova.html>

³ <https://sne.space>

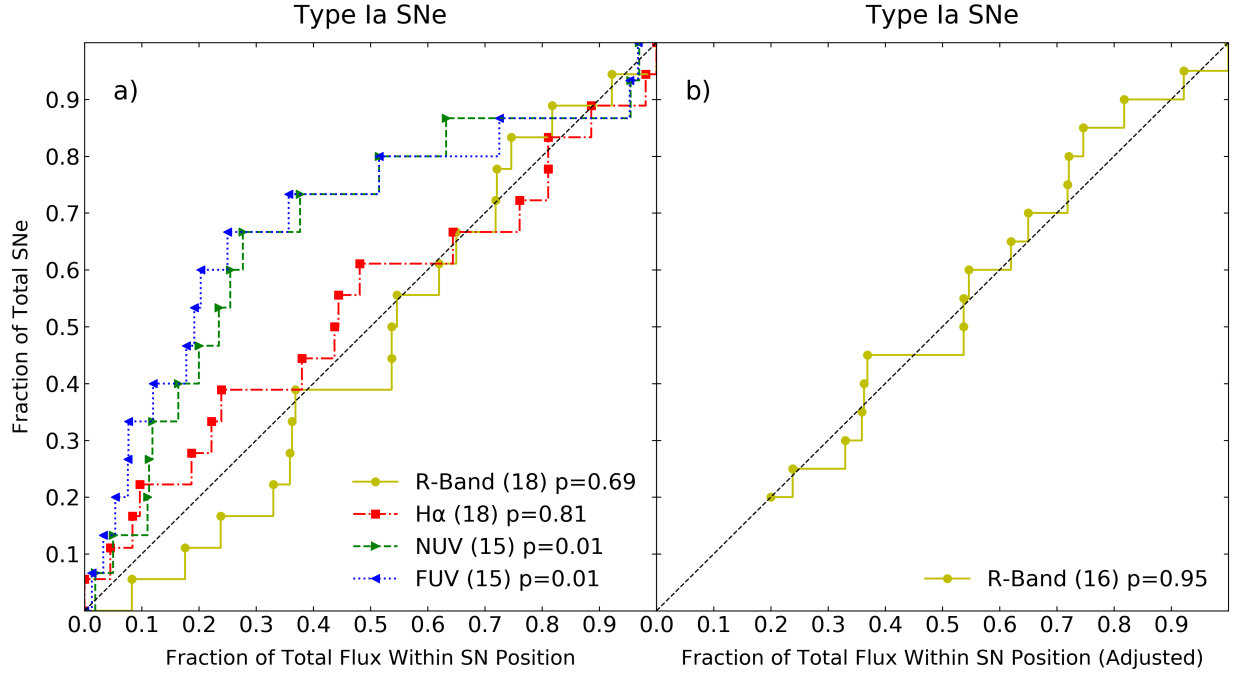


Figure 5. Cumulative distribution functions (CDFs) of the fluxes of the host galaxies interior to the Type Ia SNe positions (see Section 2.2 for method). The *R*-band, H α , NUV and FUV CDFs are shown in yellow, red, green and blue, respectively, using the symbols shown in the key. The number of SNe used in the construction of each CDF is also given in the key. The diagonal dotted normal line is an ideal 1:1 CDF where the cumulative number of Type Ia SNe exactly traces the radial flux distribution. The significance (p) of the one-tailed Kolmogorov-Smirnov (KS) testing is also listed, indicating the likelihood that the specified CDF is derived from the same population as the normal line. The Anderson-Darling test generates similar results; see Appendix A for a summary. (a) CDFs show the radial distribution of all SINGG Type Ia SNe. (b) Only Type Ia SNe occurring beyond the inner 20 per cent of the *R*-band flux distribution are included in the CDF here. This CDF commences at (0.2, 0.2); the artificial start point reflecting the 1.00 slope of the best fit line (see Section 3.1) and the extent of observed central deficits (e.g. Anderson et al. 2015b). As detailed in Section 3.1, bulges contribute significantly to central *R*-band fluxes, while producing fewer Type Ia SNe per unit mass than discs. The $p = 0.95$ result shows that the radial distribution of SINGG Type Ia SNe outside the central region is consistent with the *R*-band light distribution.

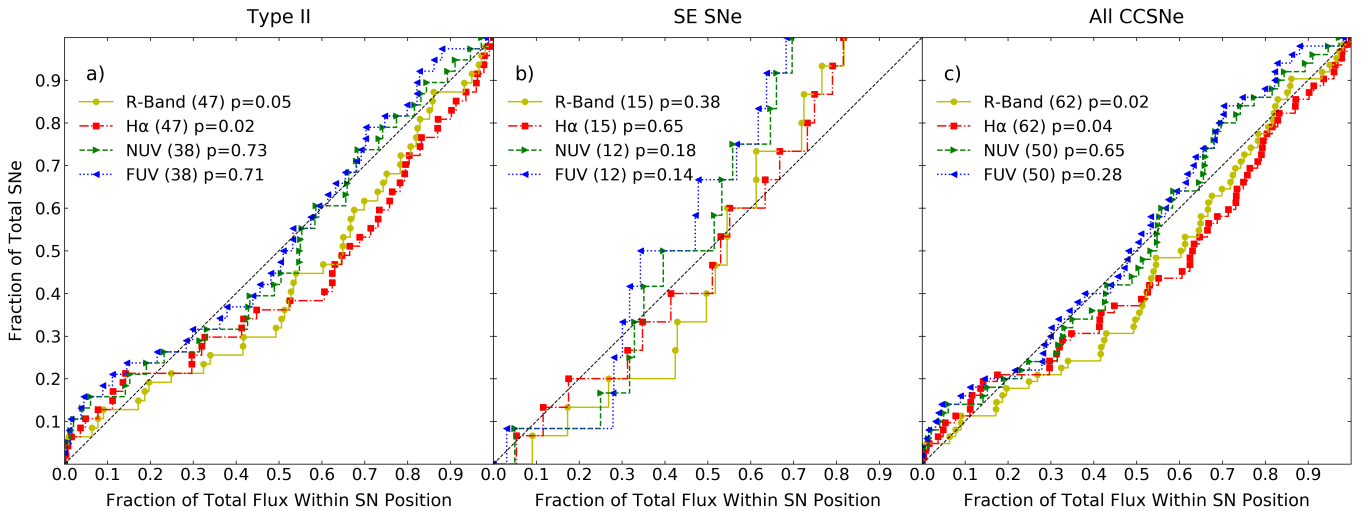


Figure 6. CDFs for (a) Type II SNe, (b) stripped-envelope supernova (SE SNe: Types Ib, Ic, Ib/c and Iib) and (c) the combined Type II and SE SNe sample. See Figure 5 for further description.

Excluding the two SINGG Type Ia SNe occurring inside the central, bulge-dominated, 20 per cent of R -band emission, Figure 5b shows that the radial distribution of the Type Ia population is strongly traced by the host galaxy's R -band emission ($p = 0.95$). Given the pivotal role of low mass WDs in all of the key models of Type Ia SNe generation (e.g. Livio & Mazzali 2018), the overall correlation of the Type Ia SN radial distribution with R -band light distribution is expected.

Our results are consistent with the findings of Anderson et al. (2015b) who found the Type Ia SNe CDF followed R -band fluxes. Their strongest correlation, however, was with B -band fluxes; this wavelength is somewhat more sensitive to high mass stars than R -band emission which traces a wide range of stellar populations and stellar masses. Kelly, Kirshner & Pahre (2008) also found Type Ia SNe most closely followed a similar wavelength (g' -band). The Type Ia SNe rate is highly dependent on global star formation, however, and is, therefore, highly dependent on the host galaxy colour, with bluer galaxies having the highest Type Ia SNe rate per unit mass (e.g. Mannucci et al. 2005; Mannucci, Della Valle & Panagia 2006). Type Ia SNe commonly occur in elliptical galaxies, including those with very little recent star formation (e.g. Oemler & Tinsley 1979; Cappellaro et al. 1999; Mannucci et al. 2005), however, showing at least some progenitors are from older stellar populations.

The radial distribution of Type Ia SNe does not correlate with the UV flux distributions at a statistically significant level (see Fig. 5a: $p = 0.01$ for both NUV and FUV), in agreement with Anderson et al. (2015b). As UV is a useful tracer of moderate to high mass stars and, therefore, also a tracer of moderate emission time-scales (e.g. Hygate et al. 2019), the divergence of the UV CDF from the dotted normal line in Figure 5a suggests that Type Ia SNe have progenitor systems from different mass and time-scale ranges.

3.2 Type II SNe

The radial distribution of Type II SNe shows strong agreement with both UV fluxes ($p = 0.73$ and 0.71 for NUV and FUV, respectively) and differs from the R -band and $H\alpha$ light distributions at, or near, statistically significant levels: $p = 0.05$ and 0.02 , respectively (see Fig. 6a and Appendix A). Type II SNe occur throughout the optical disc and examples can be found near or at $R_{\text{max,opt}}$ (see also Fig. 7e,f).

The $H\alpha$ CDF for Type II SNe (see Fig. 6a) has a central section with a reduced slope; just over 10 per cent of Type II SNe are found in 30 per cent of the flux (between 30 to 60 per cent of the total flux - see also Fig. A1b). Strong bars are known to cause a notable suppression of massive star formation in early-type spirals (see Hakobyan et al. 2016a, and references therein) and this could contribute to this CDF feature.

No Type II SNe are found in the outer ~ 30 per cent of the FUV apertures by radius (see Fig. 7g,h). This lack of Type II SNe in the outskirts could arise from a combination of Type II SN progenitors having masses towards the higher end of the mass range traced by UV and weak star formation in outer discs, apparently with an Initial Mass Function deficient in the most massive stars (e.g. Bruzese

et al. 2015; Watts et al. 2018; Bruzese et al. 2019). Metallicity gradients are unlikely to be important, with research showing that progenitor metallicity is not a significant factor in determining SN type (Anderson et al. 2010).

The physical areas beyond $R_{90,UV}$ and $R_{90,opt}$ can be sizeable; XUV discs are common (Thilker et al. 2005; Gil de Paz et al. 2005; Thilker et al. 2007, and see Fig. 2) and R -band fluxes and $H\alpha$ emission are concentrated (see the normalised radial profiles in Figs 7e,f and 4). As explained in Section 2.2, performing radial analysis within R_{90} allows the bulk of the light to be assessed while ignoring the outskirts of the host galaxies, where local environmental factors may profoundly impact star formation.

Type II SNe within R_{90} are best traced by FUV ($p = 0.52$; see Fig. 8a) and deviate from $H\alpha$, although not at a statistically significant level ($p = 0.06$). Using a much larger sample, Anderson & James (2009) also observed the positive correlation of Type II SNe and FUV and the deviation from $H\alpha$ emission.

The correlation of Type II SNe with FUV R_{90} fluxes is consistent with growing evidence that most, if not all, of Type IIP SNe originate from single moderately massive ($M_i \sim 8 - 16 M_\odot$) red supergiants (RSG) (see Smartt et al. 2002; Van Dyk 2017). However, some research suggests Type II SNe cannot arise solely from single stars (e.g. Kuncarayakti et al. 2018). There are only a few direct detections of Type IIL SN progenitors (Van Dyk 2017) and these support slightly more massive progenitors for some Type IIL SNe (Fraser et al. 2014; Groh et al. 2013b, but see Valenti et al. 2016).

The low correlation of the overall Type II SN distribution and $H\alpha$, tracer of very high mass stellar populations, is consistent with observational evidence and modelling that indicates that most very massive ($M \geq 18 M_\odot$) stars may collapse directly to a black hole (to become "failed supernovae" e.g. Fryer 1999; Smartt et al. 2009; Lovegrove & Woosley 2013; Jennings et al. 2014; Smartt 2015; Sukhbold et al. 2016; Adams et al. 2017). Adams et al. (2017) confirmed the first case of a disappearing massive star using the Large Binocular Telescope to search for failed SN candidates (N6946-BH1: Kochanek et al. 2008, and see also Reynolds, Fraser & Gilmore 2015). The $25 M_\odot$ RSG progenitor experienced considerable mass loss of its outer layers before leaving signs of a newly formed black hole (e.g. late-time emission Perna et al. 2014), without a CCSN explosion occurring. The direct-to-black-hole evolution of massive stars could explain the lack of high mass CCSN progenitors identified to date (e.g. Smartt 2015; Adams et al. 2017) and the compact remnant mass function (see Kochanek 2014). Chini et al. (2012) found most (> 82 per cent) massive stars ($M > 20 M_\odot$) are in close binary systems and this can have a profound impact on the evolution of the progenitor (see Sana et al. 2012, and references therein). Over 70 per cent, for example, will exchange mass with a companion, and very close binaries may undergo a stellar merger before ultimately collapsing directly to form a black hole (Sana et al. 2012).

3.3 High mass progenitors for stripped-envelope SNe

The radial distribution of SINGG SE SNe is best traced by the $H\alpha$ light distribution ($p = 0.65$; see Fig. 6b). This

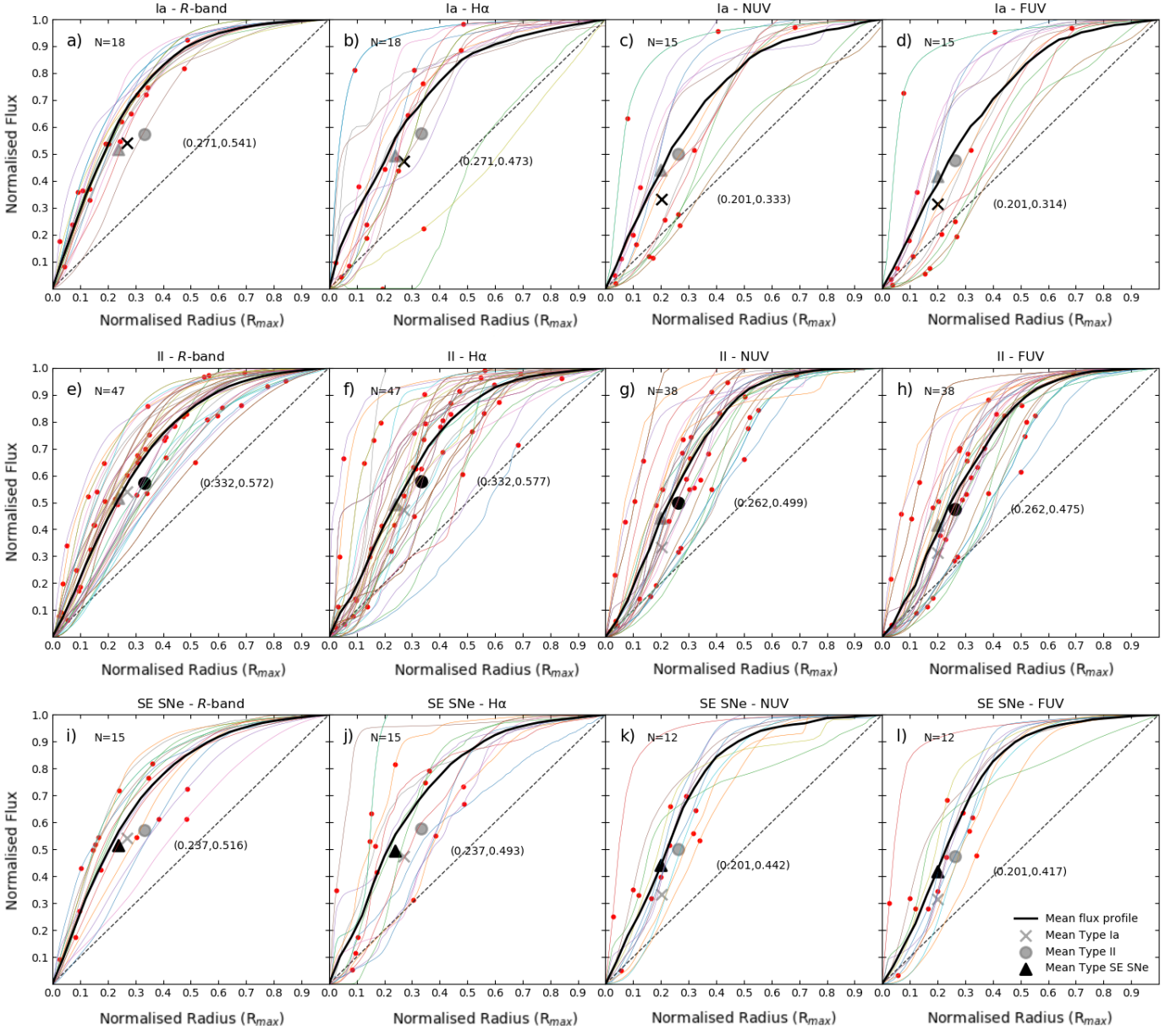


Figure 7. Normalised radial flux profiles shown as separate differently coloured lines, with SN locations indicated with small red circle(s): Type Ia SNe (top row), Type II SNe (middle row) and SE SNe (bottom row). The average radial positions for Type Ia, Type II and SE SNe are marked on each plot using a black cross, circle and triangle, respectively, and these show the now well-known centralisation of SE SNe compared to Type II SNe. To aid comparison the mean positions of the other SN types are shown with grey symbols. The lack of SE SNe in the outer regions of the UV apertures is evident in panels *k*, *l*, with no SE SNe observed in the outer ~ 30 per cent of the UV light distribution, compared to the absence of SE SNe in the outer ~ 18 per cent of the H α light distribution (panel *j*). See Sections 3.3.1 and 4.2 for further discussion.

result is consistent with SE SNe having high mass progenitors ($M_i > 20 M_\odot$) and with earlier radial analysis research (James & Anderson 2006; Anderson & James 2008; Anderson et al. 2012). The observed correlation of SE SNe with H α fluxes increases when the radial analysis is restricted to R_{90} ($p = 0.83$: see Fig. 8b), and UV fluxes improve as tracers ($p = 0.60$ and 0.43 for NUV and FUV, respectively). It is well-known that SE SNe are the CCSN subgroup most associated with high mass star-forming regions (e.g. Porter &

Filippenko 1987; Galbany et al. 2014), and Ic SNe in particular (e.g. Anderson & James 2008; Kuncarayakti et al. 2013a), implying a possible sequence of increasingly massive progenitors (II \rightarrow Ib \rightarrow Ic). Some single massive ($M_i > 25 M_\odot$) WR star SE SN progenitors have been successfully identified or modelled (e.g. Crowther 2007; Dessart et al. 2011; Mazzali et al. 2017; Prentice et al. 2018), including the first Type Ic SN progenitor identification (Van Dyk et al. 2018; Kilpatrick et al. 2018).

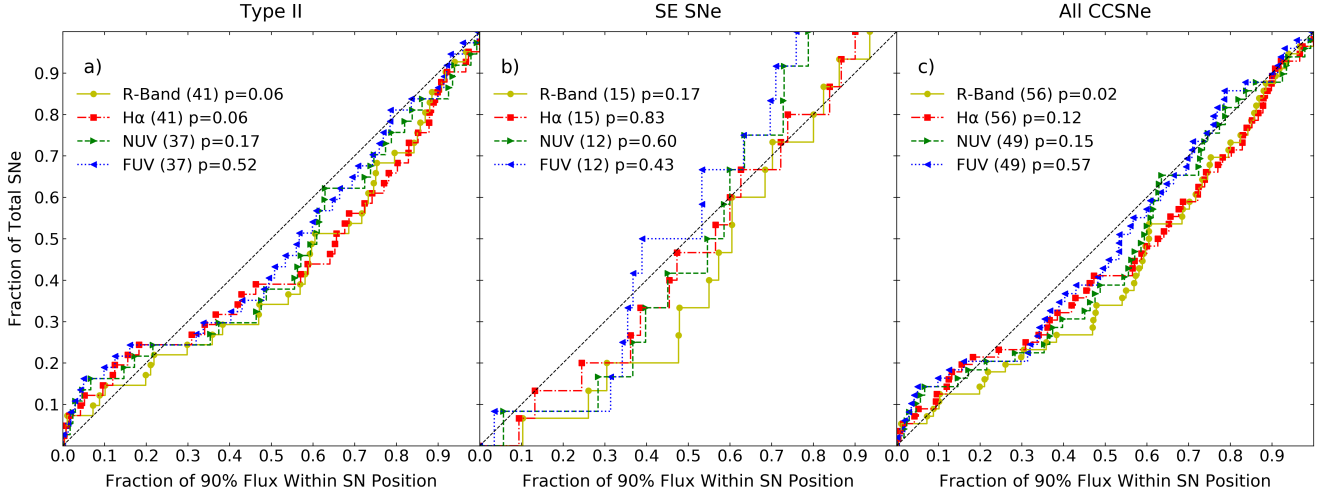


Figure 8. CDFs for SNe located within R_{90} : (a) Type II SNe, (b) stripped-envelope supernova (SE SNe: Types Ib, Ic, Ib/c and IIb) and (c) the combined Type II and SE SN sample. See Figure 5 for further description.

There is growing evidence, however, that SE SNe may have at least two progenitor streams, spanning a wide range of masses (e.g. Podsiadlowski et al. 1992; Eldridge et al. 2013; Williams et al. 2014; Ryder et al. 2018; Taddia et al. 2018; Williams et al. 2018), but see Maund (2018). Single massive star evolution models do not explain the observed ratio of SE SNe compared to Type II SNe, and a lower mass binary progenitor stream could explain the observed frequency of SE SNe (e.g. Eldridge, Izzard & Tout 2008; Smith et al. 2011a; Shivvers et al. 2017; Kilpatrick et al. 2018). Recent modelling of light curves suggests that most SE SNe have low ejecta masses ($M_{\text{ej}} = 1 - 5 M_{\odot}$), whereas massive stars typically have high ejecta masses (e.g. Lyman et al. 2016; Taddia et al. 2018). The analysis of late-phase spectra of Type IIb SNe by Jerkstrand et al. (2015) also indicates SE SNe can have moderately massive progenitors (typical $M_i \approx 12 - 16 M_{\odot}$), in line with many recent direct detections (e.g. Nomoto, Iwamoto & Suzuki 1995; Maund et al. 2004; Bersten et al. 2018).

UV fluxes are not the best tracers of the radial distribution of the SE SNe within R_{90} (see Fig. 8b). If most SE SNe are produced by lower mass stars in binary systems, as postulated by Dessart et al. (2011), then a stronger correlation would be expected, but this is not seen. Maund (2018), however, suggests very massive stars ($M_i > 30 M_{\odot}$) produce the majority of SE SNe. Using the *Hubble Space Telescope* Maund (2018) analysed the sites of 23 SE SNe, determining the age of the stellar populations remaining at the vicinity (< 150 pc) of the SN locations. Deriving stellar population ages for the resolved stars local to the SN locations using color magnitude diagrams, they find SE SNe typically to be coeval with very young stellar populations. This is indicative of much higher progenitor masses, either as single stars or in a massive binary system. Maund (2018) finds higher extinction towards the SN sites than previously assumed, thus leading to higher progenitor mass estimates.

We do not observe an excess of SE SNe near galactic centres (see Fig. 6b), unlike some observers (e.g. Anderson & James 2009; Habergham, James & Anderson 2012), but

perhaps this partially reflects the smaller size of our homogeneous sample. The SE SNe in the heterogeneous sample used by Anderson & James (2009) are significantly more centralised than our sample, as can be seen in Figure 9. Only two SE SNe (1997X and 2004dk) and two Type II SNe (1999em and 2004dg) occur in both samples; the SINGG *R*-band and $H\alpha$ enclosed flux fractions for these SNe are typically 6–12 per cent lower than the Anderson & James (2009) values, consistent with our typically larger flux apertures set to capture all detectable fluxes (see Fig. 4 and Section 2.5).

3.3.1 SE SNe absent from galaxy outskirts

The centralisation of SE SNe compared to Type II SNe noted in earlier work (e.g. van den Bergh 1997; Bartunov et al. 2007; Anderson & James 2009; Leaman et al. 2011) is evident (see Figs 6b, 7i–l, 8b). There are no SINGG SE SNe observed in the radii containing the outer ~ 30 per cent of the UV fluxes, nor in the outer ~ 18 per cent of the optical fluxes (see Fig. 7i–l). In contrast, there are no Type II SNe in the outer five to ten per cent of the UV profiles (Fig. 7g,h) while SINGG Type II SNe are located out to the full *R*-band apertures (Fig. 7e,f). Anderson & James (2009) also observed that no Type Ic SNe occurred in the outer 20 per cent of their $H\alpha$ and *R*-band flux distributions. Possible explanations for these results are discussed in Section 4.2. Recall that the large SINGG and SUNGG apertures probe the full extent of detectable fluxes (Section 2.4) and this work, therefore, examines the radial distribution of SNe well beyond the commonly used R_{25} apertures (e.g. Chakrabarti et al. 2018, and see Fig. 3).

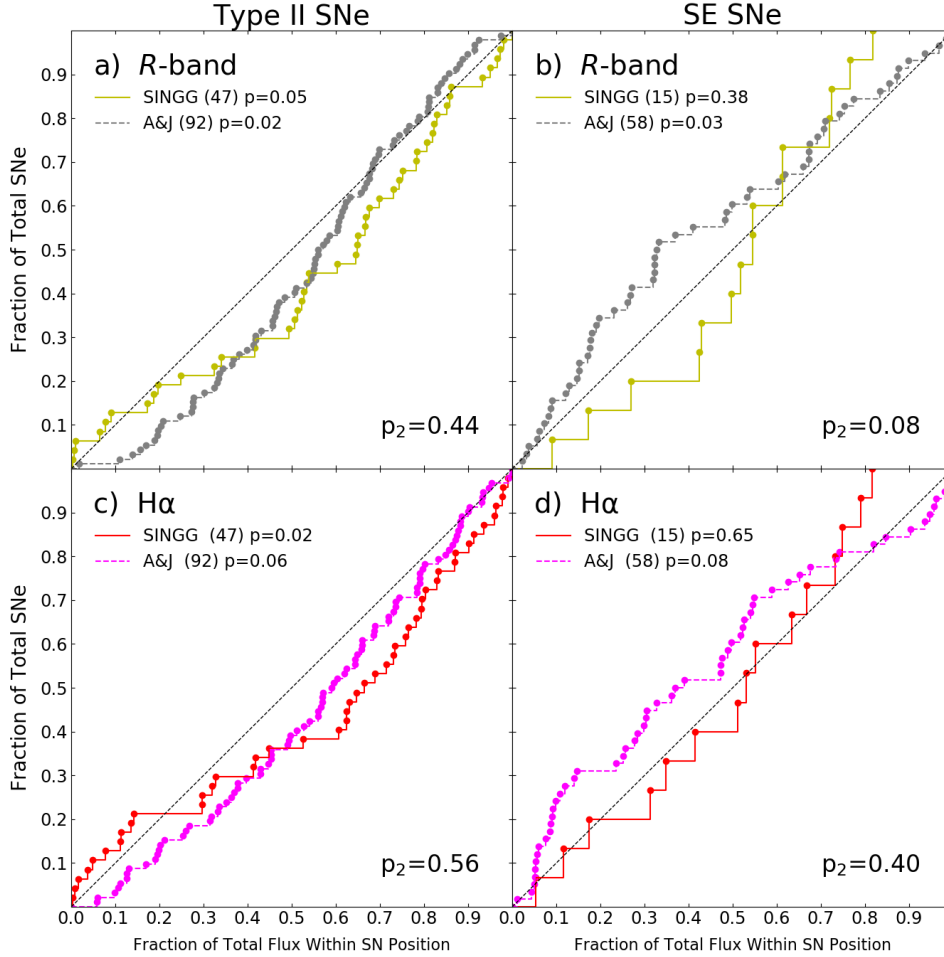


Figure 9. Comparison of the R -band and $H\alpha$ Type II SNe and SE SNe CDFs derived from the homogeneous SINGG dataset (solid lines in yellow and red for 47 Type II SNe and 15 SE SNe, respectively) with the Anderson & James (2009) sample (dashed lines in grey and magenta for 92 Type II SNe and 58 SE SNe, respectively). For consistency with SINGG, the Anderson & James (2009) sample used here excludes ten SNe which are missing either R -band or $H\alpha$ flux measurements. As in earlier CDF figures, the diagonal dotted normal line reflects an ideal 1:1 CDF where the cumulative number of the SNe exactly traces the radial flux distribution. The significance (p) of the one-tailed KS test is also listed, indicating the likelihood that the specified CDF is derived from the same population as the normal line. The significance of the two-tailed KS test (p_2) indicates the likelihood that the Anderson & James (2009) and SINGG CDFs are derived from the same population.

4 DISCUSSION

4.1 Low masses for Type Ia SNe binaries

The low likelihood that the SINGG UV light distribution and Type Ia SN radial distribution of the sample are related (Fig. 5a) suggests that at least the majority of SINGG Type Ia SNe originate from binary systems containing only low mass stars. Galactic NUV emission is a tracer of star formation out to a few ~ 100 Myr (e.g. Meurer et al. 2009), so the divergence is consistent with Type Ia SNe having older (> 100 Myr), low mass progenitors.

Our results cannot distinguish between key progenitor models that involve only low mass stars. This includes the double degenerate model (see review in Maoz, Mannucci & Nelemans 2014) and the single degenerate (SD) model case with a low mass companion (Whelan & Iben 1973). In the SD model the progenitor, a main sequence star with a mass of $M_\star < 8 M_\odot$, can evolve rapidly to form a WD of $\sim 1.4 M_\odot$ and subsequently accrete sufficient material from a non-degenerate companion, taking the primary star to, or near, the Chandrasekhar limit, causing it to explode (Hoyle & Fowler 1960). The SD model favours an initial progenitor mass range of $M_\star \sim 1.8\text{--}3 M_\odot$, while the moderately massive portion of the range ($M_\star \sim 3\text{--}8 M_\odot$) is viewed as subopti-

mal (Whelan & Iben 1973). Nomoto & Leung (2018) also suggest a potential range of companion masses ($M_{\star} \sim 0.7\text{--}6 M_{\odot}$). According to Nomoto & Leung (2018) companions within the mass range can generate the high accretion rates required for a Type Ia SN to occur and also explain the observed delay time distribution (the rate of SNe arising over time from an instantaneous burst of star formation) of Type Ia SNe (e.g. Totani et al. 2008; Maoz, Sharon & Gal-Yam 2010; Heringer, Pritchett & van Kerkwijk 2019). If correct, the SD model, together with the lack of agreement with UV fluxes, suggests the secondary stars of progenitor systems are predominately in the lower portion of the proposed $M_{\star} \sim 0.7\text{--}6 M_{\odot}$ range.

The recent increase in SN discoveries has given astronomers improved data for statistical analysis but has also revealed that over a third of Type Ia SNe are “peculiar” (e.g. Li et al. 2001; Mannucci et al. 2005, and see Taubenberger 2017 for a review). Observations have cast doubt on whether the SD model should continue to be considered the most likely (and only) progenitor model (e.g. Maoz et al. 2014; Canals, Torres & Soker 2018). Research attempting to constrain progenitors by examining spectra just days after the initial explosion for signs of interaction between the SN ejecta and companion star(s) has generated conflicting results, for example, with the signature of the hydrogen envelope of a main sequence star being detected in some cases, but not in others (e.g. Hayden et al. 2010; Brown et al. 2012; Shappee et al. 2018). Strong limits for the physical size of potential companions have been determined for a small number of cases, with most indicating that a companion, if any, must be compact (e.g. some are limited to 10 to 30 per cent of the Sun’s radius, disfavouring RSG companions and also main sequence stars (e.g. Bloom et al. 2012b; Lundqvist et al. 2015; Shappee et al. 2018). Searches for surviving companions also continue to be unsuccessful (e.g. Schaefer & Pagnotta 2012; Kerzendorf et al. 2018, but see Shen et al. 2018b). The study of detailed light curves from the recent Kepler (K2) mission is, however, providing strong constraints on possible progenitors (e.g. Dimitriadis et al. 2018).

Local environmental factors impact on Type Ia SNe, with recent work revealing that Type Ia SNe located in star forming regions have lower luminosities than their counterparts in locally passive regions (Rigault et al. 2013). The colour of Type Ia SNe also varies between SNe in the central regions and those in the outskirts of a host galaxy (Roman et al. 2018). The existing global calibrations (e.g. Hamuy et al. 1996) can, therefore, lead to bias if these local factors are not taken into account.

Type Ia progenitor models face the challenge of explaining the observed diversity of Type Ia SN events (e.g. Blondin et al. 2012), while still generating the uniformity and continuous nature of key properties, (although see Howell et al. 2006; Gall et al. 2018) that makes them such invaluable “standard candles” (Sullivan et al. 2010; Howell 2011; Maoz et al. 2014). Progenitor models must explain observations, for example, that brighter/slower Type Ia SNe are only found in star-forming galaxies while elliptical galaxies host fainter cases (e.g. Hamuy et al. 1995; Sullivan et al. 2006; Ashall et al. 2016; Graur et al. 2017). The possibility that there are multiple Type Ia SN populations (e.g. Dallaporta 1973; Della Valle & Livio 1994; Howell 2001; Mannucci

et al. 2006) requiring two or more progenitor models, is being increasingly considered (e.g. Wang & Han 2012; Wang et al. 2013; Livio & Mazzali 2018; Stritzinger et al. 2018; Bear & Soker 2018; Soker 2019). The SINGG radial analysis favours long-lived, low mass binaries for at least the majority of Type Ia progenitor systems in star-forming galaxies.

4.2 Absence of SE SNe in galaxy outskirts

The centralisation of SE SNe has previously been linked to the metallicity gradients observed in galaxies (e.g. Petrosian et al. 2005; Anderson & James 2009; Leaman et al. 2011), with central galactic locations generally having higher chemical abundances than outer regions (e.g. Henry & Worthey 1999). Metallicity drives the extent of the mass loss from winds for single massive stars, with low metallicity stars requiring higher masses than their high metallicity counterparts (e.g. Vink, de Koter & Lamers 2001; Smith 2014). On average, Type Ic SNe are located in regions of higher metallicity than Type Ib SNe (e.g. Modjaz 2012; Habergham et al. 2012) and are often located in the brightest regions of their host galaxies (e.g. Kelly et al. 2008). Others find only a weak correlation with metallicity for SE SNe compared to Type II SNe, however, and consider other factors, such as mass, binarity or disturbance, to be of greater importance (e.g. Anderson et al. 2010; Habergham et al. 2012).

Compared to other SN types, SE SNe are most associated with leading edges of spiral arms, where compression triggers star formation (e.g. Aramyan et al., 2016; Karapetyan et al. 2018). Galaxy interactions and mergers can also trigger extensive local star formation activity. SE SN centralisation is more pronounced in disturbed galaxies (e.g. Habergham et al. 2012; Anderson et al. 2015a) and galaxies with very high levels of disturbance have high SE SN to Type II SN ratios (Habergham et al. 2012). Galaxy interactions and merger activity reduce metallicity gradients compared to normal isolated galaxies (e.g. Kewley et al. 2010), implying that metallicity is not the key factor explaining the relative deficiency of SE SNe in the outskirts of galaxies.

Stellar discs typically have sharp edges when observed using broadband optical wavelengths (Kregel, Van Der Kruit & Grijs 2002; van der Kruit 2007; Meurer et al. 2018, and see Fig. 7a,e,i) and H α emission (Kennicutt 1989; Martin & Kennicutt 2001, and see Fig. 7b,f,j). Galaxies do not generally exhibit the same sharp truncation in the UV fluxes as they do in H α (Thilker et al. 2005) and many have an XUV disc (Thilker et al. 2007). The lack of SE SNe in the outskirts of galaxies is consistent with these SNe having higher mass progenitors than Type II SNe and with a reduced massive star formation efficiency (i.e. a bottom-heavy IMF) in the low density, outer regions of galaxies (e.g. Thilker et al. 2005; Bruzzone et al. 2015; Watts et al. 2018, Bruzzone et al. 2019, in prep.). Graur et al. (2017) found SE SNe under-represented by a factor of about 3 in low mass galaxies ($M < 10^{10} M_{\odot}$). Reduced massive SFEs are also found in low H I mass, low luminosity and low surface brightness galaxies (Lee et al. 2004; Hoversten & Glazebrook 2008; Meurer et al. 2009; Lee et al. 2009; Audcent-Ross et al. 2018).

5 CONCLUSIONS

We have shown that Type Ia SN progenitors in late-type galaxies are best traced by the *R*-band light distribution in the disc, i.e. after allowing for the bulge, and that there is no correlation with UV fluxes. This is consistent with most, if not all, Type Ia WD progenitors having low mass companions as proposed in the double degenerate model or, in the case of the single degenerate model, with red giant companions (Nomoto & Leung 2018). While the single degenerate model allows for higher mass main sequence sub-giant companions, our results do not support such binary systems being a major progenitor stream of Type Ia SNe.

The radial distribution of Type II SNe inside R_{90} (determined using both *R*-band and FUV) is best traced by FUV fluxes. This is consistent with a growing number of direct detections indicating that Type II SNe have moderately massive progenitors.

SE SNe have the strongest correlation with the $H\alpha$ light distribution, supporting the generally held view that they have the highest mass progenitors ($M_* \gtrsim 20 M_{\odot}$). It is not consistent, however, with the increasing number of direct detections of moderately massive binary SE SN progenitors (but see Maund 2018). At least two distinct SE SN progenitor streams, covering different mass ranges, may be required to explain these conflicting results.

The CCSN population in the homogeneous SINGG/SUNGG sample exhibit the well-known centralisation of SE SNe with respect to Type II SNe, with the outskirts of the galaxies being devoid of SE SNe; no SE SN cases occur in the outer third of the FUV fluxes, nor in the outer ~ 20 per cent of the *R*-band fluxes. The observations are consistent with high mass progenitors for SE SNe and reduced massive star formation efficiencies in the low density outskirts of galaxies.

ACKNOWLEDGEMENTS

We thank the anonymous referee for helpful and detailed comments that have improved this paper. FAR thanks J.J. Eldridge for useful discussions and comments on an earlier draft of the paper. Partial funding for the SINGG and SUNGG surveys came from NASA grants NAG5-13083 (LTSA program), GALEX GI04-0105-0009 (NASA GALEX Guest Investigator grant) and NNX09AF85G (GALEX archival grant) to G.R. Meurer. FAR acknowledges partial funding from the Department of Physics, University of Western Australia, receipt of a Student Travel Award from the Astronomical Society of Australia and financial support from the Space Telescope Science Institute (STScI) to attend the 2019 STScI Spring Symposium. This research has made use of the NASA/IPAC Extragalactic Database (NED), which is operated by the Jet Propulsion Laboratory, California Institute of Technology, under contract with the National Aeronautics and Space Administration. The IAU Central Bureau for Astronomical Telegrams database and the Open Supernova Catalog were used to identify SNe that occurred in the SINGG/SUNGG galaxies. Anderson-Darling software by SPC for Excel (<https://www.spcforexcel.com>) was used in this research.

ORCID IDS

Fiona Audcent-Ross	https://orcid.org/0000-0002-2770-8004
Gerhardt R. Meurer	https://orcid.org/0000-0002-0163-2507
Stuart D. Ryder	https://orcid.org/0000-0003-4501-8100
O. Ivy Wong	https://orcid.org/0000-0003-4264-3509
Ji Hoon Kim	https://orcid.org/0000-0002-1418-3309

REFERENCES

- Adams S. M., Kochanek C. S., Gerke J. R., Stanek K. Z., Dai X., 2017, *MNRAS*, 468, 4968
- Anderson J. P., James P. A., 2008, *MNRAS*, 390, 1527
- Anderson J. P., James P. A., 2009, *MNRAS*, 399, 559
- Anderson J. P., Covarrubias R. A., James P. A., Hamuy M., Haberman S. M., 2010, *MNRAS*, 407, 2660
- Anderson J. P., Haberman S. M., James P. A., Hamuy M., 2012, *MNRAS*, 424, 1372
- Anderson J. P., James P. A., Haberman S. M., Galbany L., Kunaravayakti H., 2015a, *PASA*, 32, 19
- Anderson J. P., James P. A., Förster F., González-Gaitán S., Haberman S. M., Hamuy M., Lyman J. D., 2015b, *MNRAS*, 448, 732
- Anderson L. D., et al., 2017, *A&A*, 605, 58
- Aramyan L. S., et al., 2016, *MNRAS*, 459, 3130
- Arcavi I., et al., 2012, *ApJ*, 756, L30
- Ashall C., Mazzali P., Sasdelli M., Prentice S. J., 2016, *MNRAS*, 460, 3529
- Audcent-Ross F. M., et al., 2018, *MNRAS*, 480, 119
- Bartunov O. S., Marakova I., Tsvetkov D., 1992, *A&A*, 264, 428
- Bartunov O. S., Tsvetkov D. Y., Pavlyuk N. N., 2007, *Highlights Astron.*, 14, 316
- Bastian N., Goodwin S. P., 2006, *MNRAS*, 369, L9
- Bastian N., Gieles M., Lamers H., Scheepmaker R., de Grijs R., 2005, *A&A*, 431, 905
- Bear E., Soker N., 2018, *MNRAS*, 480, 3702
- Begelman M. C., Sarazin C. L., 1986, *ApJ*, 302, L59
- Bekki K., 2008, *MNRAS*, 388, 10
- Bellm E. C., et al., 2019, *PASP*, 131, 018002
- Bersten M. C., et al., 2018, *Nature*, 554, 497
- Bethe H. A., Brown G. E., Applegate J., Lattimer J. M., 1979, *Nucl. Phys. A*, 324, 487
- Blondin S., et al., 2012, *AJ*, 143, 126
- Bloom J. S., et al., 2012a, *PASP*, 124, 1175
- Bloom J. S., et al., 2012b, *ApJ*, 744, L17
- Botticella M. T., Smartt S. J., Kennicutt R. C., Cappellaro E., Sereno M., Lee J. C., 2012, *A&A*, 537, A132
- Bressert E., et al., 2010, *MNRAS*, 409, L54
- Brown P. J., Dawson K. S., Harris D. W., Olmstead M., Milne P., Roming P. W. A., 2012, *ApJ*, 749, 18
- Bruzzese S. M., Meurer G. R., Lagos C. D. P., Elson E. C., Werk J. K., Blakeslee J. P., Ford H., 2015, *MNRAS*, 447, 618
- Bruzzese S. M., et al., 2019, *MNRAS*, in press
- Bushouse H., 1987, *ApJ*, 320, 49
- Canals P., Torres S., Soker N., 2018, *MNRAS*, 480, 4519
- Cappellaro E., Turatto M., Tsvetkov D. Y., Bartunov O. S., Pollas C., Evans R., Hamuy M., 1997, *A&A*, 322, 431
- Cappellaro E., Evans R., Turatto M., 1999, *A&A*, 351, 459
- Chakrabarti S., Dell B., Graur O., Filippenko A. V., Lewis B. T., McKee C. F., 2018, *ApJ*, 863
- Chandrasekhar S., 1931, *ApJ*, 74, 81

- Chini R., Hoffmeister V. H., Nasser A., Stahl O., Zinnecker H., 2012, *MNRAS*, 424, 1925
- Crockett R. M., et al., 2007, *MNRAS*, 381, 835
- Crowther P. A., 2007, *ARA&A*, 45, 177
- D'Agostino R., Stephens M., 1986, Goodness-of-fit techniques. Statistics: textbooks and monographs, M. Dekker, New York
- Dallaporta N., 1973, *A&A*, 29, 393
- Della Valle M., Livio M., 1994, *ApJ*, 423, L31
- Dessart L., Hillier D. J., Livne E., Yoon S.-C., Woosley S., Waldman R., Langer N., 2011, *MNRAS*, 414, 2985
- Dimitriadis G., et al., 2018, *ApJ*, 870, L1
- Driver S., et al., 2006, *MNRAS*, 368, 414
- Driver S. P., et al., 2018, *MNRAS*, 475, 2891
- Eldridge J. J., Izzard R. G., Tout C. A., 2008, *MNRAS*, 384, 1109
- Eldridge J. J., Fraser M., Smartt S. J., Maund J. R., Crockett R. M., 2013, *MNRAS*, 436, 774
- Eldridge J. J., Fraser M., Maund J. R., Smartt S. J., 2015, *MNRAS*, 446, 2689
- Filippenko A. V., 1997, *ARA&A*, 35, 309
- Filippenko A. V., Matheson T., Ho L. C., 1993, *ApJ*, 415, L103
- Förster F., Schawinski K., 2008, *MNRAS*, 388, L74
- Fraser M., et al., 2014, *MNRAS*, 439, L56
- Freeman K. C., 1970, *ApJ*, 160, 811
- Fryer C. L., 1999, *ApJ*, 522, 413
- Fryer C. L., et al., 2010, *ApJ*, 725, 296
- Gal-Yam A., 2016, arXiv:, 1611.09353
- Gal-Yam A., Mazzali P. A., Manulis I., Bishop D., 2013, *PASP*, 125, 749
- Galbany L., et al., 2014, *A&A*, 572, 38
- Gall C., et al., 2018, *A&A*, 611, 58
- Gaskell C. M., Cappellaro E., Dinerstein H. L., Garnett D. R., Harkness R. P., Wheeler J. C., 1986, *ApJ*, 306, L77
- Gil de Paz A., et al., 2005, *ApJ*, 627, L29
- Gogarten S. M., Dalcanton J. J., Murphy J. W., Williams B. F., Gilbert K., Dolphin A., 2009, *ApJ*, 703, 300
- Goldstein D. A., Kasen D., 2018, *ApJ*, 852, L33
- Gonzalez-Gaitan S., et al., 2015, *MNRAS*, 451, 2212
- Graur O., Bianco F. B., Modjaz M., Shivvers I., Filippenko A. V., Li W., Smith N., 2017, *ApJ*, 837, 121
- Groh J. H., Meynet G., Ekström S., 2013a, *A&A*, 550, L7
- Groh J. H., Meynet G., Georgy C., Ekström S., 2013b, *A&A*, 558, 131
- Guillochon J., Parrent J., Kelley L. Z., Margutti R., 2017, *ApJ*, 835, 64
- Habergham S. M., James P. A., Anderson J. P., 2012, *MNRAS*, 424, 2841
- Hachisu I., Kato M., Saio H., Nomoto K., 2012, *ApJ*, 744, 69
- Hakobyan A. A., et al., 2016a, *MNRAS*, 456, 2848
- Hakobyan A. A., et al., 2016b, arXiv:, 1609.08319
- Hakobyan A. A., et al., 2017, *MNRAS*, 471, 1390
- Hamuy M., Phillips M. M., Maza J., Suntzeff N. B., Schommer R. A., Aviles R., 1995, *AJ*, 109, 1
- Hamuy M., Phillips M. M., Suntzeff N. B., Schommer R. A., Maza J., Aviles R., 1996, *AJ*, 112, 2391
- Han Z., Podsiadlowski P., 2004, *MNRAS*, 350, 1301
- Hanish D. J., et al., 2006, *ApJ*, 649, 150
- Hayden B. T., et al., 2010, *ApJ*, 722, 1691
- Heger A., Jeannin L., Langer N., Baraffe I., 1997, *A&A*, 327, 224
- Heger A., Fryer C. L., Woosley S. E., Langer N., Hartmann D. H., 2003, *ApJ*, 591, 288
- Henry R., Worthey G., 1999, *PASP*, 111, 919
- Heringer E., Pritchett C., van Kerkwijk M. H., 2019, *ApJ*, 882, 52
- Hillebrandt W., Niemeyer J. C., 2000, *ARA&A*, 38, 191
- Horiuchi S., Beacom J. F., Kochanek C. S., Prieto J. L., Stanek K. Z., Thompson T. A., 2011, *ApJ*, 738, 154
- Hoversten E. A., Glazebrook K., 2008, *ApJ*, 675, 163
- Howell D. A., 2001, *ApJ*, 554, L193
- Howell D. A., 2011, *Nature Commun.*, 2, 350
- Howell D. A., et al., 2006, *Nature*, 443, 308
- Hoyle F., Fowler W. A., 1960, *ApJ*, 132, 565
- Hygate A. P. S., Kruijssen J. M. D., Chevance M., Schruha A., Haydon D. T., Longmore S. N., 2019, *MNRAS*, 488, 2800
- Iben I. J., Tutukov A. V., 1984, *ApJS*, 54, 335
- Ivanov V. D., Hamuy M., Pinto P. A., 2000, *ApJ*, 542, 588
- James P. A., Anderson J. P., 2006, *A&A*, 453, 57
- Jencson J. E., et al., 2019, arXiv:, 1901.00871
- Jennings Z. G., Williams B. F., Murphy J. W., Dalcanton J. J., Gilbert K. M., Dolphin A. E., Weisz D. R., Fouesneau M., 2014, *ApJ*, 795, 170
- Jerkstrand A., Ergon M., Smartt S. J., Fransson C., Sollerman J., Taubenberger S., Bersten M., Spyromilio J., 2015, *A&A*, 573, 12
- Johnson H. M., MacLeod J. M., 1963, *PASP*, 75, 123
- Karapetyan A. G., Hakobyan A. A., Barkhudaryan L. V., Mamon G. A., Kunth D., Adibekyan V., Turatto M., 2018, *MNRAS*, 481, 566
- Kelly P. L., Kirshner R. P., Pahre M., 2008, *ApJ*, 687, 1201
- Kenney J. D. P., Tal T., Crowl H. H., Feldmeier J., Jacoby G. H., 2008, *ApJ*, 687, L69
- Kennicutt R. C. J., 1989, *ApJ*, 344, 685
- Kerzendorf W. E., Strampelli G., Shen K. J., Schwab J., Pakmor R., Do T., Buchner J., Rest A., 2018, *MNRAS*, 479, 192
- Kewley L. J., Rupke D., Jabran Zahid H., Geller M. J., Barton E. J., 2010, *ApJ*, 721, L48
- Kilpatrick C. D., et al., 2018, *MNRAS*, 480, 2072
- Kochanek C. S., 2014, *ApJ*, 785, 28
- Kochanek C. S., Beacom J. F., Kistler M. D., Prieto J. L., Stanek K. Z., Thompson T. A., Yüksel H., 2008, *ApJ*, 684, 1336
- Kool E. C., et al., 2018, *MNRAS*, 473, 5641
- Koribalski B. S., et al., 2004, *AJ*, 128, 16
- Kotak R., Vink J. S., 2006, *A&A*, 460, L5
- Kregel M., Van Der Kruit P. C., Grijs R. d., 2002, *MNRAS*, 334, 646
- Kuncarayakti H., et al., 2013a, *AJ*, 146, 30
- Kuncarayakti H., et al., 2013b, *AJ*, 146, 31
- Kuncarayakti H., et al., 2018, *A&A*, 613, 35
- Lada C. J., Lada E. A., 2003, *ARA&A*, 41, 57
- Larson R. B., 1976, *MNRAS*, 176, 31
- Leaman J., Li W., Chornock R., Filippenko A. V., 2011, *MNRAS*, 412, 1419
- Lee J. H., Lee M. G., 2014, *ApJ*, 786, 130
- Lee H.-C., Gibson B. K., Flynn C., Kawata D., Beasley M. A., 2004, *MNRAS*, 353, 113
- Lee J. C., Kennicutt R. C., José G. Funes S. J., Sakai S., Akiyama S., 2009, *ApJ*, 692, 1305
- Lennarz D., Altmann D., Wiebusch C., 2012, *A&A*, 538, A120
- Li W., Filippenko A. V., Treffers R. R., Riess A. G., Hu J., Qiu Y., 2001, *ApJ*, 546, 734
- Livio M., Mazzali P., 2018, *Phys. Rep.*, 736, 1
- Lovegrove E., Woosley S. E., 2013, *ApJ*, 769, 109
- Lundqvist P., et al., 2015, *A&A*, 577, 39
- Lyman J. D., Bersier D., James P. A., Mazzali P. A., Eldridge J. J., Fraser M., Pian E., 2016, *MNRAS*, 457, 328
- Lyman J. D., et al., 2018, *MNRAS*, 473, 1359
- Magnier E. A., et al., 2013, *ApJS*, 205, 20
- Mannucci F., Della Valle M., Panagia N., Cappellaro E., Cresci G., Maiolino R., Petrosian A., Turatto M., 2005, *A&A*, 433, 807
- Mannucci F., Della Valle M., Panagia N., 2006, *MNRAS*, 370, 773
- Maoz D., Sharon K., Gal-Yam A., 2010, *ApJ*, 722, 1879
- Maoz D., Mannucci F., Nelemans G., 2014, *ARA&A*, 52, 107
- Martin C. L., Kennicutt J. R. C., 2001, *ApJ*, 555, 301
- Masci F. J., et al., 2017, *PASP*, 129, 014002
- Mattila S., et al., 2012, *ApJ*, 756, 111
- Maund J. R., 2018, *MNRAS*, 476, 2629

- Maund J. R., Smartt S. J., Kudritzki R. P., Podsiadlowski P., Gilmore G. F., 2004, *Nature*, 427, 129
- Mazzali P. A., Sauer D. N., Pian E., Deng J., Prentice S., Ben Ami S., Taubenberger S., Nomoto K., 2017, *MNRAS*, 469, 2498
- Meurer G. R., et al., 2006, *ApJS*, 165, 307
- Meurer G. R., et al., 2009, *ApJ*, 695, 765
- Meurer G. R., Obreschkow D., Wong O. I., Zheng Z., Audcent-Ross F. M., Hanish D. J., 2018, *MNRAS*, 476, 1624
- Meyer M. J., et al., 2004, *MNRAS*, 350, 1195
- Minkowski R., 1941, *PASP*, 53, 224
- Modjaz M., 2012, *Proc. IAU*, 7, 207
- Morselli L., Popesso P., Erfanianfar G., Concas A., 2017, *A&A*, 597, 97
- Nomoto K., 1982, *ApJ*, 253, 798
- Nomoto K., Leung S.-C., 2018, *Space Sci. Rev.*, 214, 67
- Nomoto K., Thielemann F. K., Yokoi K., 1984, *ApJ*, 286, 644
- Nomoto K., Iwamoto K., Suzuki T., 1995, *Phys. Rep.*, 256, 173
- Oemler A. J., Tinsley B. M., 1979, *AJ*, 84, 985
- Patterson F., 1940, *Harv. Coll. Obs. Bull.*, 914, 9
- Peletier R. F., Balcells M., 1996, *AJ*, 111, 223
- Perna R., Duffell P., Cantiello M., MacFadyen A. I., 2014, *ApJ*, 781, 119
- Petrosian A., et al., 2005, *AJ*, 129, 1369
- Phillips M. M., Lira P., Suntzeff N. B., Schommer R. A., Hamuy M., Maza J., 1999, *AJ*, 118, 1766
- Podsiadlowski P., Joss P. C., Hsu J. J. L., 1992, *ApJ*, 391, 246
- Portegies Zwart S. F., McMillan S. L. W., Gieles M., 2010, *ARA&A*, 48, 431
- Porter A. C., Filippenko A. V., 1987, *AJ*, 93, 1372
- Prentice S. J., et al., 2018, *MNRAS*, 478, 4162
- Reynolds T. M., Fraser M., Gilmore G., 2015, *MNRAS*, 453, 2885
- Riess A. G., et al., 1998, *AJ*, 116, 1009
- Rigault M., et al., 2013, *A&A*, 560, A66
- Roman M., et al., 2018, *A&A*, 615, 68
- Roškar R., Debattista V. P., Stinson G. S., Quinn T. R., Kaufmann T., Wadsley J., 2008, *ApJ*, 675, L65
- Ryder S. D., et al., 2018, *ApJ*, 856, 83
- Sana H., et al., 2012, *Science*, 337, 444
- Sancisi R., Fraternali F., Oosterloo T., van der Hulst T., 2008, *A&AR*, 15, 189
- Sanders N. E., et al., 2015, *ApJ*, 799, 208
- Schaefer B. E., Pagnotta A., 2012, *Nature*, 481, 164
- Shappee B. J., Piro A. L., Stanek K. Z., Patel S. G., Margutti R. A., Lipunov V. M., Pogge R. W., 2018, *ApJ*, 855, 6
- Shen K. J., Kasen D., Miles B. J., Townsley D. M., 2018a, *ApJ*, 854, 52
- Shen K. J., et al., 2018b, *ApJ*, 865, 15
- Shivvers I., et al., 2017, *PASP*, 129, 4201
- Smartt S. J., 2015, *PASA*, 32, 22
- Smartt S. J., Gilmore G. F., Tout C. A., Hodgkin S. T., 2002, *ApJ*, 565, 1089
- Smartt S. J., Eldridge J. J., Crockett R. M., Maund J. R., 2009, *MNRAS*, 395, 1409
- Smith L. F., 1968, *MNRAS*, 141, 317
- Smith N., 2014, *ARA&A*, 52, 487
- Smith N., Owocki S. P., 2006, *ApJ*, 645, L45
- Smith N., Li W., Filippenko A. V., Chornock R., 2011a, *MNRAS*, 412, 1522
- Smith N., Gehrz R. D., Campbell R., Kassis M., Le Mignant D., Kulohiwa K., Filippenko A. V., 2011b, *MNRAS*, 418, 1959
- Smith N., Mauerhan J. C., Prieto J. L., 2014, *MNRAS*, 438, 1191
- Soker N., 2019, *MNRAS*, 490, 2430
- Stoner E. C., 2011, *Philos. Mag.*, 91, 3423
- Stritzinger M. D., et al., 2018, *ApJ*, 864, L35
- Sukhbold T., Ertl T., Woosley S. E., Brown J. M., Janka H. T., 2016, *ApJ*, 821, 38
- Sullivan M., Treyer M. A., Ellis R. S., Bridges T. J., Milliard B., Donas J., 2000, *MNRAS*, 312, 442
- Sullivan M., et al., 2006, *ApJ*, 648, 868
- Sullivan M., et al., 2010, *MNRAS*, 406, 782
- Taddia F., et al., 2018, *A&A*, 609, 136
- Taubenberger S., 2017, *The Extremes of Thermonuclear Supernovae*. Springer International Publishing AG, doi:10.1007/978-3-319-21846-5-37
- Thilker D. A., et al., 2005, *ApJ*, 619, L79
- Thilker D. A., et al., 2007, *ApJS*, 173, 538
- Totani T., Morokuma T., Oda T., Doi M., Yasuda N., 2008, *PASJ*, 60, 1327
- Tsvetkov D. Y., Pavlyuk N. N., Bartunov O. S., 2004, *Astron. Lett.*, 30, 729
- Valenti S., et al., 2016, *MNRAS*, 459, 3939
- Van Dyk S. D., 2017, *Philos. Trans. Royal Soc.*, 375, 2016277
- Van Dyk S. D., et al., 2018, *ApJ*, 860, 90
- Vink J. S., de Koter A., Lamers H. J. G. L. M., 2001, *A&A*, 369, 574
- Vučetić M. M., Arbutina B., Urošević D., 2015, *MNRAS*, 446, 943
- Wang B., Han Z., 2012, *New Astron. Rev.*, 56, 122
- Wang L., Höflich P., Wheeler J. C., 1997, *ApJ*, 483, L29
- Wang X., Wang L., Filippenko A. V., Zhang T., Zhao X., 2013, *Science*, 340, 170
- Wang J., et al., 2018, *MNRAS*, 479, 4292
- Watts A. B., Meurer G. R., Lagos C. D. P., Bruzese S. M., Kroupa P., Jerabkova T., 2018, *MNRAS*, 477, 5554
- Webbink R. F., 1984, *ApJ*, 277, 355
- Whelan J., Iben Icko J., 1973, *ApJ*, 186, 1007
- Whipple F. L., 1939, *Proc. Natl. Acad. Sci. USA*, 25, 118
- Williams B. F., Peterson S., Murphy J., Gilbert K., Dalcanton J. J., Dolphin A. E., Jennings Z. G., 2014, *ApJ*, 791, 105
- Williams B. F., Hillis T. J., Murphy J. W., Gilbert K., Dalcanton J. J., Dolphin A. E., 2018, *ApJ*, 860, 39
- Wong O. I., 2007, *Phd*, Univ. Melbourne
- Wong O. I., Meurer G. R., Zheng Z., Heckman T. M., Thilker D. A., Zwaan M. A., 2016, *MNRAS*, 460, 1106
- Zheng Z., et al., 2015, *ApJ*, 800, 120
- Zwaan M. A., et al., 2004, *MNRAS*, 350, 1210
- van den Bergh S., 1997, *AJ*, 113, 197
- van der Kruit P. C., 2007, *A&A*, 466, 883

APPENDIX A: ENCLOSED FLUX FRACTION HISTOGRAMS

Figure A1 provides an alternative to the CDF presentation of the radial distribution of SNe used in the body of this paper and reinforces its results. The lack of Type II and SE SNe in the outskirts of the UV radial flux distributions of our sample is particularly evident in Fig. A1c,d, for example.

The statistical significance of our results using Kolmogorov-Smirnov (KS) testing are detailed in the body of this paper. The Anderson-Darling (AD) test (case 3, D'Agostino & Stephens 1986) was also used to examine the significance of our results and generated results consistent with the KS testing. The radial distribution of Type II SNe over the full apertures is not consistent with either *R*-band and *H α* radial fluxes (Anderson-Darling $AD^* > \sim 2$ and $p_{AD} = 0.0$), while NUV has the only non-negligible p_{AD} value ($AD^* = 0.6$ and $p_{AD} = 0.12$). In statistically significant results, albeit with small numbers of SNe, the radial distribution of the 18 Type Ia SNe over the full apertures is not consistent with UV radial fluxes (Anderson-Darling $AD^* > 3$ and $p_{AD} = 0.0$) and is consistent with *R*-band fluxes ($AD^* = 0.13$ and $p_{AD} = 0.98$), while only *H α* fluxes may trace the 15 SE SNe ($AD^* = 0.53$ and $p_{AD} = 0.18$),

with all other radial fluxes being statistically rejected ($AD^* > 1$ and $p_{AD} \leq 0.01$).

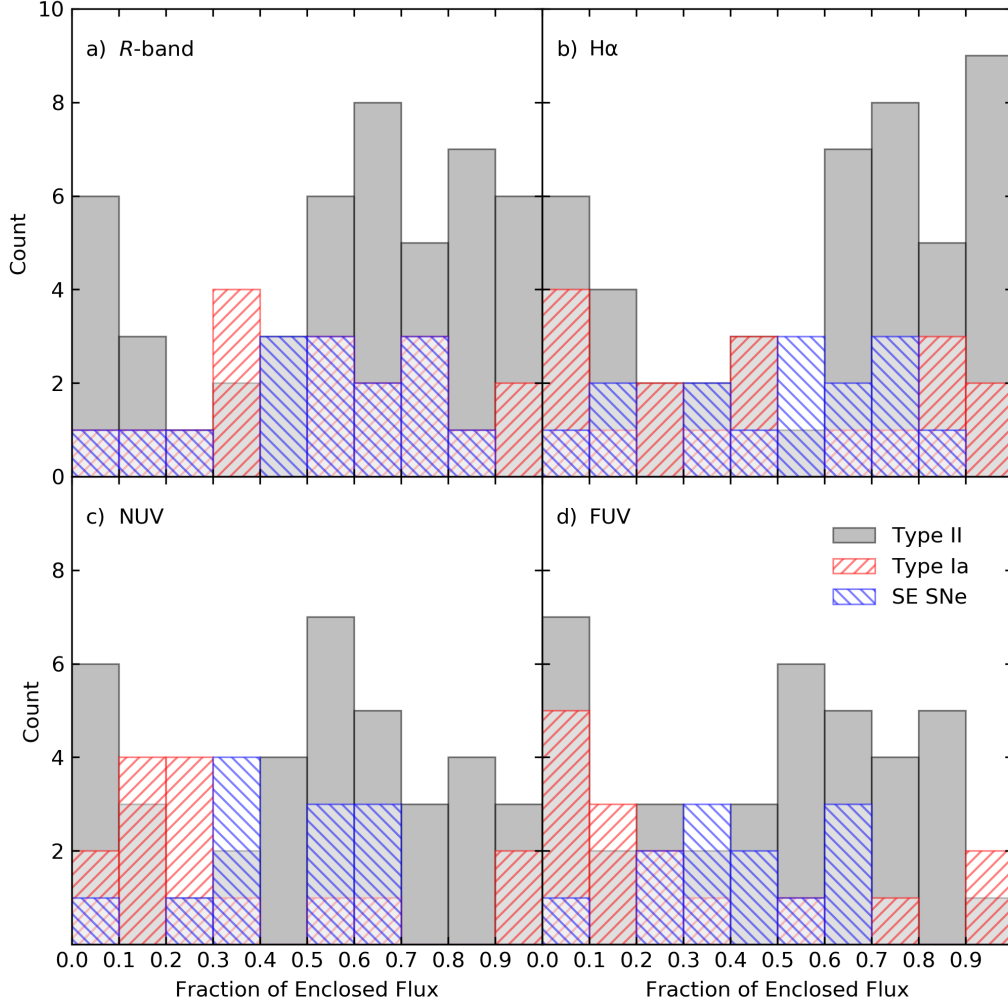


Figure A1. Histograms of the radial enclosed flux fractions (see Section 2.2 for method). This figure is an alternative representation of the results in Figures 5a and 6a,b, and similarly illustrates, for example, a central deficit of Type Ia SNe and the lack of Type II and SE SNe in the outskirts of the UV flux distributions of our sample. Type II SNe are indicated with solid grey, Type Ia with red upward-slanting lines, and SE SNe with blue downward-slanting lines (as shown in the key above).